Journal of Materials Chemistry A

PAPER

View Article Online
View Journal | View Issue

Cite this: J. Mater. Chem. A, 2014, 2, 15448

One-pot synthesis of a nitrogen and phosphorus-dual-doped carbon nanotube array as a highly effective electrocatalyst for the oxygen reduction reaction†

Jinliang Zhu,[a] San Ping Jiang,*[b] Ruihong Wang,[c] Keying Shi[c] and Pei Kang Shen*[a]

Received 14th May 2014
Accepted 29th July 2014

DOI: 10.1039/c4ta02427c

www.rsc.org/MaterialsA

A nitrogen and phosphorus-dual-doped carbon nanotube (N, P-CNT) array has been successfully synthesized by a novel one-pot method, using an aminophosphonic acid resin as the N, P and C sources. The N, P-CNTs are open with large inner channels, allowing oxygen molecules to access a large number of catalytically active sites on the inner walls. The N, P-CNTs are not only comparable to Pt/C in electrocatalytic activity for the oxygen reduction reaction (ORR) in 0.1 M KOH, but are also highly stable and tolerant to methanol and CO poisoning. An onset potential of 0.95 V close to that of Pt/C and a well-defined limiting current plateau for the ORR are observed. Moreover, there is almost no visible current density decrease on N, P-CNTs after 5000 cycles.

1 Introduction

Considerable efforts have been devoted to synthesize hollow nanostructured carbon materials such as fullerenes,[1] carbon nanotubes,[2,3] nanoshells,[4] carbon nanocages[5] and nanocones[6] for their specific architectures and unique physical and chemical properties. Carbon nanotubes (CNTs), one of the most important hollow nanostructured carbon materials, exhibit potential applications in hydrogen storage,[7] lithium-ion batteries (LIBs),[8] supercapacitors,[9] nanocontainers and nanoreactors[10,11] and fuel cells.[12,13] It has been reported that carbon materials doped by heteroatoms such as nitrogen, boron, phosphorus, sulfur and fluorine have high electrocatalytic activity, high durability and high tolerance towards poisoning of the oxygen reduction reaction.[14–18] Dai *et al.*[3] showed that nitrogen-doped CNT (N-CNT) arrays have high electrocatalytic activity for the oxygen reduction reaction (ORR) in alkaline solutions. Recently, Dai *et al.*[15] demonstrated that CNT arrays co-doped with N and P have significantly enhanced electrocatalytic activity towards ORR, compared with CNTs doped by N or P only, due to a synergetic effect. Doping with heteroatoms can modulate the structure, electronic and physicochemical properties of carbon materials like CNTs. For example, the incorporation of nitrogen atoms into CNTs can activate the π electrons of carbon by conjugation with the lone-pair electrons of N dopants and significantly increase active sites for the ORR.[19,20] The ORR at the cathode of fuel cells plays a key role in the performance of the fuel cells.

Doping CNTs by N or P can be achieved *via* '*in situ*' doping and 'post-synthesis treatment' methods.[21,22] However, for *in situ* doping methods, such as arc-discharge, CVD and laser ablation, special instrumentation or rigorous condition control is often required.[21,23,24] The method of post-synthesis treatment requires toxic nitrogen precursors (*e.g.*, NH_3).[21] Moreover, the ORR activities of the majority of reported N-CNTs are still not satisfactory as compared to Pt-based catalysts. Architecture or nanostructure of CNTs plays an important role in the electrocatalytic activity of N-CNTs. For example, N-CNTs[25,26] and N, P-dual-doped CNTs,[15,27] having a bamboo-like structure and nodes, could reduce the catalytic active sites in inner walls by blocking their access to oxygen molecules. On the other hand, less catalytically active sites may lead to a two-electron oxygen reduction pathway, forming intermediate H_2O_2 species, which reduces the electrocatalytic efficiency as well as the stability of catalysts.[28] Therefore, it is of scientific and technological importance to develop novel and facile strategies to synthesize N and P-dual-doped CNTs with a robust nano-structure for enhanced activities and durability for ORR.

Herein, for the first time, we report a facile and one-pot synthesis of a nitrogen and phosphorus-dual-doped carbon nanotube (N, P-CNT) array with simultaneous nitrogen and

[a]State Key Laboratory of Optoelectronic Materials and Technologies, Key Laboratory of Low-carbon Chemistry & Energy Conservation of Guangdong Province, School of Physics and Engineering, Sun Yat-sen University, 135 Xingang Road, Guangzhou, 510275, P. R. China. E-mail: stsspk@mail.sysu.edu.cn; Fax: +8620-84036736; Tel: +8620-84036736

[b]Fuels and Energy Technology Institute & Department of Chemical Engineering, Curtin University, Perth, WA6102, Australia. E-mail: s.jiang@curtin.edu.au

[c]Key Laboratory of Functional Inorganic Material Chemistry, Ministry of Education of the People's Republic of China, Heilongjiang University, Harbin, 150080, P. R. China

† Electronic supplementary information (ESI) available. See DOI: 10.1039/c4ta02427c

phosphorus doping by pyrolysis of nitrogen and phosphorus-containing resin in the presence of nickel foam. Due to the available catalytic active sites in the inner walls and the synergetic effect arising from co-doping CNTs with both P and N, the N, P-CNT array shows superior ORR activity with respect to bamboo-like N-CNTs. The N, P-CNT catalyst provides sufficient catalytically active sites, therefore showing an excellent electrocatalytic performance and stability for ORR in an alkaline medium.

2 Experimental section

2.1 Synthesis of the N, P-CNT array

The as-received aminophosphonic acid resin (APAR, Sunresin New Materials Co. Ltd., China) was cleaned with deionized water and then dried before using. The treated resin (1.5 g) was placed in a clean quartz boat and the boat was capped with a nickel foam. The boat was then heated to 850 °C at a heating rate of 3 °C min^{-1} and held for 30 min in a tube furnace in a N_2 atmosphere. After cooling down to room temperature, the nickel foam was treated with diluted hydrochloric acid to remove nickel substrates and then the N, P-CNTs were collected. The N-doped CNTs (N-CNTs) were also synthesized for comparison. Commercial carbon nanotubes (CNTs) with a purity of >95% (Shenzhen Nanotech Co., Ltd., China) and Pt/C (46.7 wt% Pt, TKK, Japan) catalysts were used as received.

2.2 Physical characterization

The Raman spectroscopic measurements were carried out on a Raman spectrometer (Renishaw Corp., UK) using a He–Ne laser with a wavelength of 514.5 nm. The X-ray photoelectron spectroscopy (XPS) measurements were performed in an ESCALAB 250 spectrometer under vacuum (about 2×10^{-9} mbar). Monochromatic Al Kα (150 W, 1486.6 eV) was used as the excitation source. All the binding energies were calibrated with respect to the C1s peak at 284.8 eV. The morphology characterizations were performed on a scanning electron microscope (SEM) (Quanta 400 FEG, FEI Company). The transmission electron microscopy (TEM) and element mapping investigations were carried out on a JEOL JEM-2010 (JEOL Ltd.) operating at 200 kV and a FEI Tecnai G2 F30.

2.3 Electrochemical characterization

The performance of the N, P-CNTs for ORR was measured on a rotating ring-disk electrode (RRDE) with a bipotentiostat (Pine Instrument Co., USA) in a three-electrode cell by using a reversible hydrogen electrode (RHE) as the reference electrode, and a graphite electrode as the counter electrode. The working electrode was a rotating ring/disk electrode with a glassy carbon disk (5.61 mm in diameter). 5.0 mg of N, P-CNTs (N-CNTs or CNTs) was added into 1.9 mL ethanol and 0.1 mL Nafion solution (5 wt%, DuPont, USA) and ultrasonicated for 30 min to form a well-dispersed ink. The ink (100 μL) was transferred onto the surface of the glass carbon electrode and then dried under an infrared lamp for 5 min to obtain a catalyst thin film. The total Pt loadings were controlled at 0.0101 mg cm^{-2}. The ORR tests were performed with a scan rate of 5 mV s^{-1} in an O_2-saturated 0.1 mol L^{-1} KOH solution at 25 °C. The rotating speed was controlled at 1600 rpm. In the RRDE tests, the ring potential was set to 1.2 V *vs.* RHE.

3 Results and discussion

Fig. 1 and S1 (ESI†) show the principle of the growth process of the N, P-CNT array, using an aminophosphonic acid resin (APAR) precursor. The APAR precursor was decomposed in N_2 at 325 °C, providing nitrogen, phosphorus and hydrocarbon sources for the growth of the N, P-CNT array (Fig. 1a). As the temperature rose, the released phosphorus species reacted with clean nickel foam (Fig. 1b and e), forming rod-like Ni_2P particles[29,30] on the surface of the nickel foam (Fig. 1c and f). The rod-like Ni_2P particles served as seeds to catalyze the growth of carbon nanotubes (Fig. 1d and g). As the Ni_2P catalyst particles are most likely located at the tips of carbon tubes, the growth process may follow the 'adsorption-diffusion-precipitation model' in the CVD method using metal particles as catalysts.[31,32] The hydrocarbons released by the resin would adsorb on the surface of Ni_2P particles and the carbon diffusion and consequent precipitation would lead to the growth of carbon nanotubes with simultaneous doping of N and P. Such a simultaneous growth mechanism of N, P-CNTs is further confirmed by the element mapping investigations (Fig. 2). Ni and P are mainly accumulated at the tip of the tube (Fig. 2), indicating that nickel was pulled away from the Ni foam substrate by the formation of Ni_2P seeds, which is confirmed by XRD in Fig. S2.† The uniform distribution of N and to a lesser

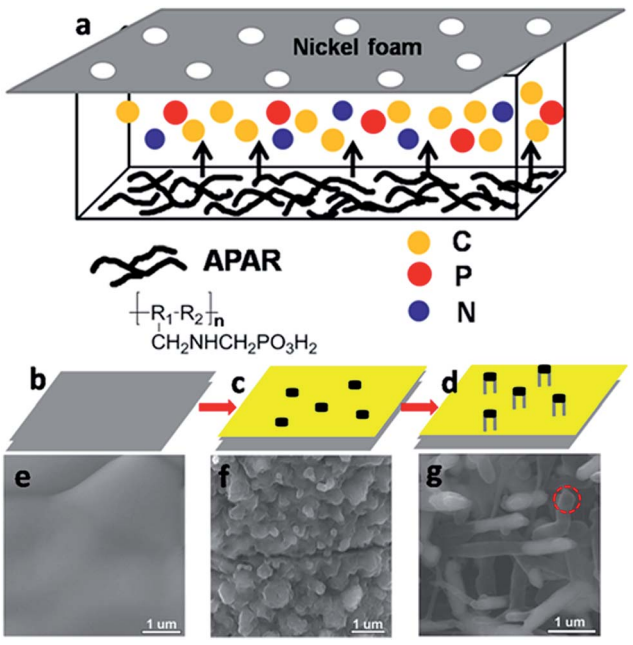

Fig. 1 Schematic illustration of the growth process of the N, P-CNT array and SEM images of growing N, P-CNTs at different stages (a), arrangement of the APAR and Ni foam as substrate, (b and e), initial Ni foam substrate, (c and f), Ni foam at 850 °C for 1 min and (d and g), Ni foam at 850 °C for 15 min.

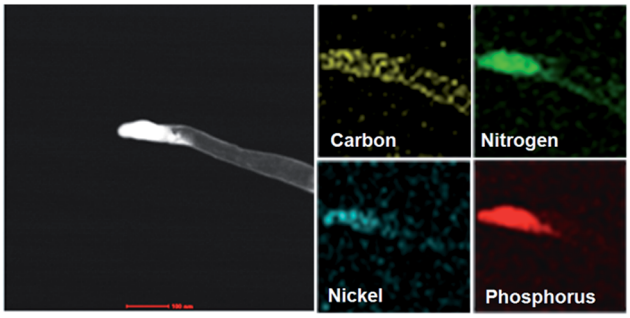

Fig. 2 TEM image (the bar is 100 nm) and corresponding element mappings of a growing N, P-CNT.

degree of P along the carbon tubes confirms the simultaneous doping of N and P during the growth of the carbon tubes.

The production of high-density rod-like Ni_2P particles with uniform size is critical to the growth of the N, P-CNT array. It is very different from bamboo-like N-CNTs, where asymmetric metal catalyst particles would lead to the accumulation of carbon at graphite-catalyst edges and consequently the formation of nodes,[33–35] since the cylindrical Ni_2P rod catalysts avoid the formation of nodes. This is indicated by the growth of very uniform and hollow N, P-CNTs (Fig. 1g). The one-pot synthesis strategy designed for the growth of N, P-CNT arrays has significant advantages over conventional *in situ* doping or post-synthesis methods. First, the use of APAR provides a low-cost and environmentally friendly carbon, nitrogen and phosphorus source, and requires no special instruments or rigorous conditions. Second, the rod-like Ni_2P particles as catalyst seeds are formed *in situ* and high density and uniform formation of such rod-like seeds prevent formation of bamboo-like structure and nodes. Third, P and N atoms are simultaneously incorporated into the CNTs during the tube growth, eliminating post-synthesis or extra doping processes.

As shown in the inset of Fig. 3a, the nickel foam substrates are covered with compact and uniform N, P-CNTs, and form a coral-like array. The magnified SEM images show that the N, P-CNT has a noodle-like shape and a length of 20–30 micrometers (Fig. S3†). The N, P-CNTs are vertically aligned, and some adjacent N, P-CNTs may be in contact along the length of the array. The N, P-CNTs show a bigger tube with diameter of about 100–200 nm (Fig. 3a and c), as compared to the conventional multi-walled carbon nanotubes (MWCNTs).[36,37] The N, P-CNT array formed by the one-pot synthesis method is also characterized by an open-ended structure (Fig. 3c). It can be observed that there are defects and distortions in the carbon lattice of the wall, as shown in Fig. 3d. The wall thickness of the tube is about 4.5 nm and the ratio of internal diameter to wall thickness can be as high as 20. In contrast, the synthesized N-CNTs show a typical bamboo-like structure as shown in Fig. 4. The SEM image of the N-CNTs indicates that the N-CNTs grow randomly. A thick wall and nodes can be clearly observed in the TEM image of a single N-CNT.

Fig. 5a shows the Raman spectra of N, P-CNTs and N-CNTs in the range of 500–2500 cm^{-1}. The band observed at about

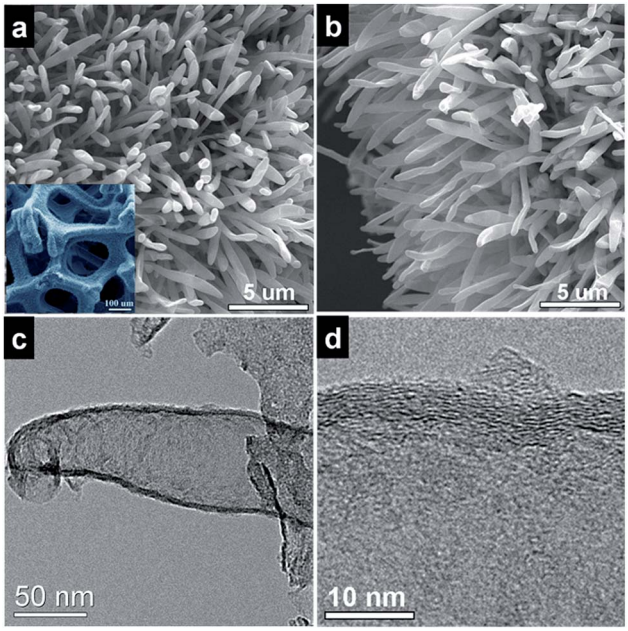

Fig. 3 SEM and TEM images of the N, P-CNT array: (a) top view and (b) side view. (c) TEM and (d) HRTEM images of an individual N, P-CNT. The inset in (a) shows an overall view of the N, P-CNTs.

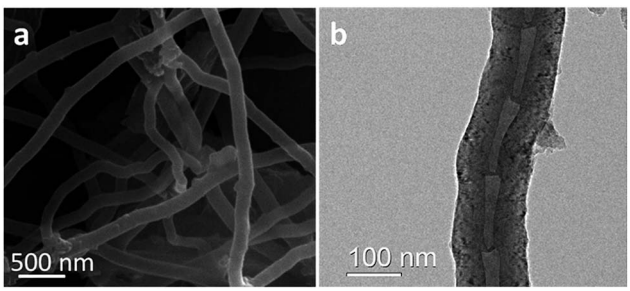

Fig. 4 SEM and TEM images of the N-CNTs.

1358 cm^{-1} is assigned to the D-band, which originates from defects in the hexagonal sp^2 carbon network. The band appearing at 1580 cm^{-1} is assigned to the G-band, reflecting the structural intensity of the sp^2-hybridized carbon atom.[38,39] The intensity ratio of the G-band to D-band (I_G/I_D) is approximately 1.18, which is a little lower than that of N-CNTs. It may be attributable to the doping with P, which can induce defect sites and destruction in the carbon lattice, and lead to an increase in the degree of distortion.

Fig. 5b and d show N1s spectra of the N-CNTs and N, P-CNTs, respectively, which can be further deconvoluted into three peaks:[40,41] the peak at 398.7 eV can be attributed to pyridinic nitrogen, which is bonded to two carbon atoms and exists on the edge of graphite planes. The peaks located at 399.6 and 401.2 eV can be assigned to pyrrolic nitrogen and graphitic nitrogen, respectively. The pyridinic-N with a lone electron pair in the plane of the carbon matrix induces the side-on adsorption during chemisorption of oxygen on the surface of the catalyst, which effectively weakens the O–O bond and facilitates

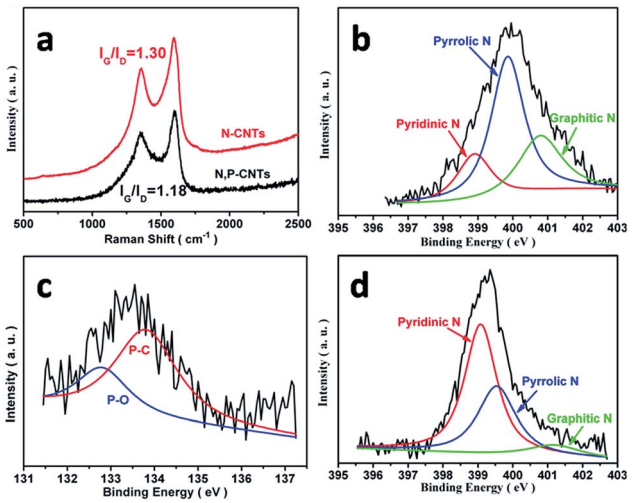

Fig. 5 (a) Raman spectra of the N, P-CNTs and N-CNTs, (b) XPS-N1s spectrum of the N-CNTs, (c) XPS-P2p and (d) XPS-N1s spectrum of the N, P-CNTs.

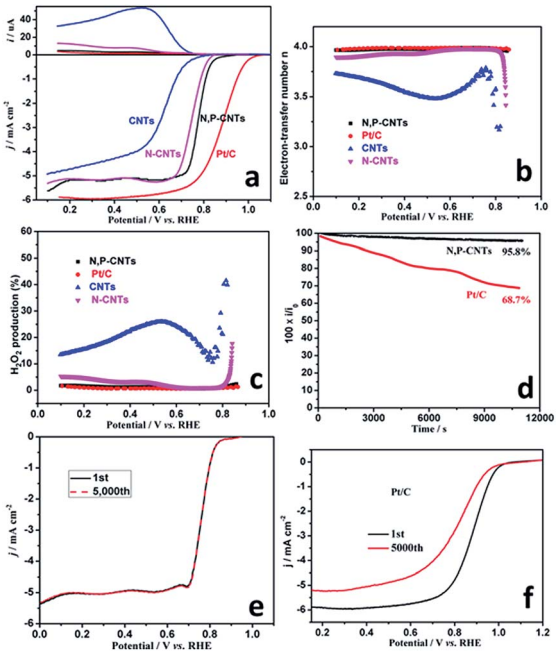

Fig. 6 (a) The linear sweep curves (down) of the catalysts on RDE for ORR and corresponding ring currents (up) at 1600 rpm in O_2-saturated 0.1 mol L^{-1} KOH at 25 °C with a sweep rate of 5 mV s^{-1}, (b) electron-transfer number *n* of the catalysts at different potentials, (c) calculated H_2O_2 production yields of the catalysts, (d) constant potential polarization curves of the N, P-CNTs and Pt/C at constant potential of 0.7 V *vs.* RHE and (e and f) ORR performance of the N, P-CNTs and Pt/C before and after 5000 cycles in 0.1 mol L^{-1} KOH.

the reduction of O_2.[42,43] The graphitic nitrogen atoms could also be ORR-active and catalyze the ORR through a direct four-electron pathway. The N1s peak clearly shifts to a lower binding energy from N-CNTs to N, P-CNTs, which is attributed to the electron transfer to N which increases the electron density on N due to the high electron-donating ability of P. The P2p spectrum of N, P-CNTs (Fig. 5c) can be resolved into two different peaks at the binding energies of 132.8 and 134.0 eV, corresponding to P–O and P–C respectively.[44,45] The N and P doping levels of N-CNTs to N, P-CNTs are shown in Table 1. Phosphorus, one of the N-group elements, shows similar chemical properties to N and leads to synergistic effects between the dopants.[46,47] P, with a larger atomic radius and higher electron-donating ability, tends to induce more defects and structural corruption, which increases active sites for ORR and improves electrocatalytic activity.[45,48]

The electrocatalytic activities of as-synthesized N, P-CNTs for the oxygen reduction reaction are shown in Fig. 6 and S4.† For the purpose of comparison, the performances of N-CNTs, commercial CNTs and Pt/C (46.7 wt% Pt, TKK, Japan) catalysts for ORR are also given. The ring current increases dramatically on CNTs in the oxygen reduction potential region (Fig. 6a), which indicates more HO_2^- generated by a two-electron reduction of oxygen. However, the ring current is negligible for the ORR on N, P-CNTs. The onset potential of N, P-CNTs is 0.95 V *vs.* RHE, very close to the onset potential of the Pt/C catalyst. Most importantly, the half wave potential of the reaction on the N, P-CNTs is 0.79 V *vs.* RHE, almost the same as that on the Pt/C catalyst (0.795 V). The remarkable electrocatalytic activity of N, P-CNTs for ORR is not only attributable to N, P-dual doping, which can change the net charge of adjacent carbon atoms to facilitate the ORR, but also to its unique architecture. The open-ended N, P-CNT has a large number of hollow channels and inner walls, which increase the active sites compared with bamboo-shaped N-doped CNT.

Table 1 XPS analysis of the samples

Sample	Nitrogen (at. %)	Phosphorus (at. %)
N-CNTs	4.90	0
N, P-CNTs	4.17	4.28

As shown in Fig. 6b and c, the electron-transfer number *n* and H_2O_2 production yields of the CNTs, N-CNTs, N, P-CNTs and Pt/C during the ORR can be calculated according to the following equations:[49]

$$n = \frac{4I_D}{I_D + (I_R/N)}$$

$$\%H_2O_2 = 100\frac{(4-n)}{2}$$

where *n* is the apparent electron-transfer number and $\%H_2O_2$ is the percentage of the electron used to generate the H_2O_2 during the ORR. I_D is the absolute value of the Faradaic current at the disk, I_R is the absolute value of the ring current and *N* is the collection efficiency. Obviously, the *n* value was calculated to be from 3.95 to 3.97 and the H_2O_2 produced is below 3% at potentials from 0.1 V to 0.85 V *vs.* RHE, indicating a high selectivity of O_2 reduction to H_2O through a four-electron route on the N, P-CNTs, similar to that on Pt/C catalysts. The CNT and

N-CNT catalysts showed more H_2O_2 generated, especially at high potentials. The stability of the N, P-CNT and Pt/C catalysts were evaluated by chronoamperometric experiments at 0.7 V *vs.* RHE (Fig. 6d). Based on the normalized current plots, the loss in the current density for the ORR on N, P-CNTs is only 4.2% after 3 h polarization, while Pt/C lost 31.3%. After continuous potential cycling, there is no visible current density decrease on N, P-CNTs after 5000 cycles (Fig. 6e), indicating the high durability of N, P-CNTs as ORR catalysts. However, a significant decrease in current density and an obvious shift in half wave potential (Fig. 6f) are observed on the Pt/C catalyst. This further indicates that N, P-CNTs have superior ORR stability compared with Pt/C catalysts.

We further evaluate the stability of the N, P-CNT catalyst by an accelerated test in the same media. After 2500 pulse potential cycles (30–60 s alternatively at 0.65 and 1.05 V/RHE) in 0.1 mol L^{-1} KOH, very little decrease in current density and almost no shift in half wave potential were observed on the N, P-CNT catalyst, indicating that the N, P-CNTs are very stable for ORR (Fig. 7).

The N, P-CNT catalyst also shows remarkable resistance and tolerance towards methanol and poisoning species of CO for ORR compared to Pt/C (Fig. 8). The Pt/C shows a significant current decay with the addition of CO into the electrolyte. However, in the case of N, P-CNTs, the effect of addition of CO on the polarization current is negligible (Fig. 8a). Similar results are observed for the introduction of methanol into the solution for ORR. Upon addition of 1.0 mol methanol to the O_2-saturated solution, a sharp positive current increase occurs on Pt/C catalysts, indicating a rapid decay in activity (Fig. 8b). However, the change in the current density is negligible for the ORR on the N, P-CNTs after the introduction of methanol.

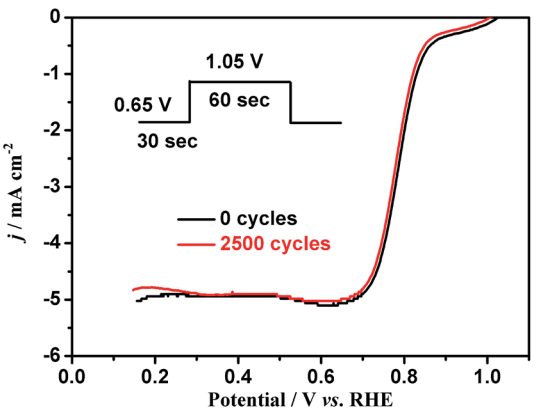

Fig. 7 The stability test of the N, P-CNT catalyst.

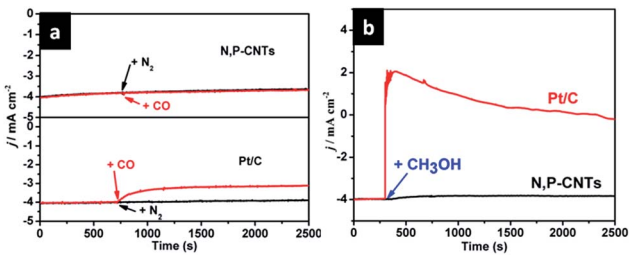

Fig. 8 (a) Constant potential polarization curves of the N, P-CNTs and Pt/C at 0.7 V *vs.* RHE in O_2-saturated 0.1 mol L^{-1} KOH solution with addition of N_2 (black line) and CO (red line) and (b) with addition of 1.0 mol methanol.

4 Conclusions

In summary, we have successfully demonstrated a novel one-pot approach to synthesize a N, P-dual-doped CNT array as a highly active electrocatalyst for ORR. The N, P-CNTs with open ends and large hollow channels provide a large number of catalytic active sites in inner walls, allowing the access of oxygen molecules. This significantly advantageous architecture is superior as compared with conventional bamboo-shaped N-CNTs and bamboo-shaped N, P-dual-doped CNTs. The comparable activity and much better methanol and CO tolerance for ORR as compared to Pt/C catalysts can be attributed to both the synergistic effect of N and P doping and the unique architecture of the N, P-CNT array. This construction of a robust CNT nanostructure for the designed electrocatalytic application and other potential applications will attract broad interest in scientific and industrial fields.

Acknowledgements

This work was supported by the Major International (Regional) Joint Research Project (51210002), the Link Project of the National Natural Science Foundation of China and Guangdong Province (U1034003), the National Natural Science Foundation of China (21073241, 21201058) and the Australian Research Council (DP120102325 and DP120104932).

Notes and references

1 D. M. Guldi, *Chem. Commun.*, 2000, 321.
2 D. Tasis, N. Tagmatarchis, A. Bianco and M. Prato, *Chem. Rev.*, 2006, **106**, 1105.
3 K. Gong, F. Du, Z. Xia, M. Durstock and L. Dai, *Science*, 2009, **323**, 760.
4 M. Matsui, N. Takahashi and J.-i. Ozaki, *Carbon*, 2011, **49**, 4505.
5 S. J. Teng, J. N. Wang and X. X. Wang, *J. Mater. Chem.*, 2011, **21**, 5443.
6 U. N. Maiti, S. Maiti, N. S. Das and K. K. Chattopadhyay, *Nanoscale*, 2011, **3**, 4135.
7 B. Assfour, S. Leoni, G. Seifert and I. A. Baburin, *Adv. Mater.*, 2011, **23**, 1237.
8 B. J. Landi, M. J. Ganter, C. D. Cress, R. A. DiLeo and R. P. Raffaelle, *Energy Environ. Sci.*, 2009, **2**, 638.
9 N. Jha, P. Ramesh, E. Bekyarova, M. E. Itkis and R. C. Haddon, *Adv. Energy Mater.*, 2012, **2**, 438.
10 H. Orikasa, N. Inokuma, S. Ittisanronnachai, X.-H. Wang, O. Kitakami and T. Kyotani, *Chem. Commun.*, 2008, 2215.
11 R. Kitaura, N. Imazu, K. Kobayashi and H. Shinohara, *Nano Lett.*, 2008, **8**, 693.

12 C. Xiong, Z. Wei, B. Hu, S. Chen, L. Li, L. Guo, *et al.*, *J. Power Sources*, 2012, **215**, 216.
13 Z. Jin, H. Nie, Z. Yang, J. Zhang, Z. Liu, X. Xu, *et al.*, *Nanoscale*, 2012, **4**, 6455.
14 L. Yang, S. Jiang, Y. Zhao, L. Zhu, S. Chen, X. Wang, *et al.*, *Angew. Chem.*, 2011, **123**, 7270.
15 D. Yu, Y. Xue and L. Dai, *J. Phys. Chem. Lett.*, 2012, **3**, 2863.
16 D. Geng, Y. Chen, Y. Chen, Y. Li, R. Li, X. Sun, *et al.*, *Energy Environ. Sci.*, 2011, **4**, 760.
17 X. Sun, Y. Zhang, P. Song, J. Pan, L. Zhuang, W. Xu, *et al.*, *ACS Catal.*, 2013, **3**, 1726.
18 Z. Yang, Z. Yao, G. Li, G. Fang, H. Nie, Z. Liu, *et al.*, *ACS Nano*, 2011, **6**, 205.
19 B. Shan and K. Cho, *Chem. Phys. Lett.*, 2010, **492**, 131.
20 Y. Tan, C. Xu, G. Chen, X. Fang, N. Zheng and Q. Xie, *Adv. Funct. Mater.*, 2012, **22**, 4584.
21 Y. Zheng, Y. Jiao, M. Jaroniec, Y. Jin and S. Z. Qiao, *Small*, 2012, **8**, 3550.
22 Y. Zhao, L. Yang, S. Chen, X. Wang, Y. Ma, Q. Wu, *et al.*, *J. Am. Chem. Soc.*, 2013, **135**, 1201.
23 Z. Wang, R. Jia, J. Zheng, J. Zhao, L. Li, J. Song, *et al.*, *ACS Nano*, 2011, **5**, 1677.
24 S. Lim, H. Elim, X. Gao, A. Wee, W. Ji, J. Lee, *et al.*, *Phys. Rev. B: Condens. Matter Mater. Phys.*, 2006, **73**, 045402.
25 T. Sharifi, G. Hu, X. Jia and T. Wågberg, *ACS Nano*, 2012, **6**, 8904.
26 L. Feng, Y. Yan, Y. Chen and L. Wang, *Energy Environ. Sci.*, 2011, **4**, 1892.
27 E. Cruz-Silva, D. A. Cullen, L. Gu, J. M. Romo-Herrera, E. Muñoz-Sandoval, F. López-Urías, *et al.*, *ACS Nano*, 2008, **2**, 441.
28 Y. Zhang, J. Ge, L. Wang, D. Wang, F. Ding, X. Tao, *et al.*, *Sci. Rep.*, 2013, **3**, 2771.
29 L. Song, S. Zhang and Q. Wei, *J. Solid State Chem.*, 2011, **184**, 1556.
30 R. Scholder, A. Apel and H. Haken, *Z. Anorg. Allg. Chem.*, 1937, **232**, 1.
31 Z. Zhu, Y. Lu, D. Qiao, S. Bai, T. Hu, L. Li, *et al.*, *J. Am. Chem. Soc.*, 2005, **127**, 15698.
32 J. P. Tessonnier and D. S. Su, *ChemSusChem*, 2011, **4**, 824.
33 X. Wu, Y. Tao, Y. Lu, L. Dong and Z. Hu, *Diamond Relat. Mater.*, 2006, **15**, 164.
34 M. Lin, J. P. Y. Tan, C. Boothroyd, K. P. Loh, E. S. Tok and Y.-L. Foo, *Nano Lett.*, 2007, **7**, 2234.
35 S. Trasobares, O. Stephan, C. Colliex, W. Hsu, H. Kroto and D. Walton, *J. Chem. Phys.*, 2002, **116**, 8966.
36 M. B. Jakubinek, M. A. White, G. Li, C. Jayasinghe, W. Cho, M. J. Schulz, *et al.*, *Carbon*, 2010, **48**, 3947.
37 M. He, S. Vasala, H. Jiang, M. Karppinen, E. I. Kauppinen, M. Niemelä, *et al.*, *Carbon*, 2012, **50**, 4750.
38 K. Ghosh, M. Kumar, T. Maruyama and Y. Ando, *Carbon*, 2009, **47**, 1565.
39 J. Zhu, Y. Li, S. Kang, X. We and P. K. Shen, *J. Mater. Chem. A*, 2014, **2**, 3142.
40 H.-P. Cong, P. Wang, M. Gong and S.-H. Yu, *Nano Energy*, 2014, **3**, 55.
41 C. H. Choi, M. W. Chung, S. H. Park and S. I. Woo, *RSC Adv.*, 2013, **3**, 4246.
42 Y. Shao, S. Zhang, M. H. Engelhard, G. Li, G. Shao, Y. Wang, *et al.*, *J. Mater. Chem.*, 2010, **20**, 7491.
43 J. Zhu, C. He, Y. Li, S. Kang and P. K. Shen, *J. Mater. Chem. A*, 2013, **1**, 14700.
44 O. S. Panwar, M. A. Khan, M. Kumar, S. M. Shivaprasad, B. S. Satyanarayana, P. N. Dixit, *et al.*, *Jpn. J. Appl. Phys.*, 2009, **48**, 5501.
45 D.-S. Yang, D. Bhattacharjya, S. Inamdar, J. Park and J.-S. Yu, *J. Am. Chem. Soc.*, 2012, **134**, 16127.
46 S. Wang, E. Iyyamperumal, A. Roy, Y. Xue, D. Yu and L. Dai, *Angew. Chem., Int. Ed.*, 2011, **50**, 11756.
47 J. Zhu and P. K. Shen, *RSC Adv.*, 2013, **3**, 14686.
48 Z. W. Liu, F. Peng, H. J. Wang, H. Yu, W. X. Zheng and J. Yang, *Angew. Chem.*, 2011, **123**, 3315.
49 G. He, Z. Yan, X. Ma, H. Meng, P. K. Shen and C. Wang, *Nanoscale*, 2011, **3**, 3578.